THE JOURNAL OF BIOLOGICAL CHEMISTRY VOL. 285, NO. 53, pp. 41533–41540, December 31, 2010

Substoichiometric Levels of Cu^{2+} Ions Accelerate the Kinetics of Fiber Formation and Promote Cell Toxicity of Amyloid-β from Alzheimer Disease*[S]

Received for publication, August 3, 2010, and in revised form, October 14, 2010 Published, JBC Papers in Press, October 25, 2010, DOI 10.1074/jbc.M110.171355

Claire J. Sarell, Shane R. Wilkinson, and John H. Viles[1]

From the School of Biological and Chemical Sciences, Queen Mary University of London, Mile End Road, London E1 4NS, United Kingdom

A role for Cu^{2+} ions in Alzheimer disease is often disputed, as it is believed that Cu^{2+} ions only promote nontoxic amorphous aggregates of amyloid-β (Aβ). In contrast with currently held opinion, we show that the presence of substoichiometric levels of Cu^{2+} ions in fact doubles the rate of production of amyloid fibers, accelerating both the nucleation and elongation of fiber formation. We suggest that binding of Cu^{2+} ions at a physiological pH causes Aβ to approach its isoelectric point, thus inducing self-association and fiber formation. We further show that Cu^{2+} ions bound to Aβ are consistently more toxic to neuronal cells than Aβ in the absence of Cu^{2+} ions, whereas Cu^{2+} ions in the absence of Aβ are not cytotoxic. The degree of Cu-Aβ cytotoxicity correlates with the levels of Cu^{2+} ions that accelerate fiber formation. We note the effect appears to be specific for Cu^{2+} ions as Zn^{2+} ions inhibit the formation of fibers. An active role for Cu^{2+} ions in accelerating fiber formation and promoting cell death suggests impaired copper homeostasis may be a risk factor in Alzheimer disease.

Alzheimer disease (AD)[2] is characterized by extracellular amyloid plaques, composed predominantly of fibrillar amyloid-β peptide (Aβ), a 39–43-residue peptide. Genetic alterations underlying familial AD are associated with mutations or increased production of Aβ, indicating that Aβ plays a central role in the disease (1).

A notable characteristic of AD is altered metal ion concentrations in the brain and disrupted metal ion homeostasis (2). Cu^{2+} ions are found concentrated within senile plaques of AD patients directly bound to Aβ (3–5). Recent *in vivo* studies using a *Drosophila* model of AD have shown that impaired copper homeostasis enhances the toxic effects of Aβ (6). Furthermore, copper in a cholesterol high diet induces amyloid plaques and learning deficits in a rabbit model of AD (7). Other *in vivo* studies have shown that copper homeostasis can influence AD pathology. In contrast to the *Drosophila* model, transgenic mice have shown a reduced AD pathology with increased intracellular copper levels (8–10).

Although studies of Aβ neurotoxicity suggest that small diffusible oligomers, rather than mature amyloid fibers, are the more toxic form (11, 12), there remains strong evidence suggesting that amyloid plaques, or possibly intermediates of the fibrils, are critical in neuronal toxicity (13, 14). Aβ oligomers may be precursors of fiber formation and may also arise from fiber fragmentation. Alternatively, oligomers may be in competition with fiber formation. Both possibilities require the self-association of monomeric Aβ, and thus factors that affect fibrillization will also influence oligomer generation.

The mechanism by which Aβ is toxic is hotly debated (11, 15). It has been proposed that Aβ can form ion channels or pores or can thin the membrane, all of which will cause membrane leakage and loss of cellular Ca^{2+} ion homeostasis. One popular hypothesis is that the membrane integrity is compromised by lipid peroxidation from reactive oxygen species, which is a key feature of the pathogenesis of AD (16, 17). It is well established that hydrogen peroxide mediates Aβ toxicity and the antioxidant enzyme catalase protects cells from Aβ toxicity (18–20). A likely source of extracellular H_2O_2 is from the Fenton redox cycling of copper or iron ions (17). We and others have shown that Cu^{2+} bound to Aβ will readily generate hydroxyl radicals and H_2O_2 in the presence of a physiological reductant such as ascorbate (19, 21–23). Indeed, transfer of Cu^{2+} from Aβ to the redox-inactive metallothionein III removes Aβ toxic properties (24).

The three histidine residues within Aβ peptide form a tetragonal complex with Cu^{2+} ions (25–35; for review, see 36, 37). Recent studies point to a dynamic Cu^{2+} complex involving imidazole coordination in both the axial and equatorial plain (25, 27, 35). A full (1:1) stoichiometric complement will bind to both monomeric and mature Aβ fibers with identical coordination geometry and affinity (25). Affinity measurements of the Cu^{2+}-Aβ complex have been revised, indicating a considerably tighter affinity than previously believed, setting the conditional dissociation constant, pH 7.4, at 60×10^{-12} M (25). Extracellular monomeric Aβ levels are thought to be 5 nM (38), whereas Aβ levels are higher in plaques and at the synapse. Furthermore, extracellular Cu^{2+} levels in the brain interstitial fluid are 100 nM. A picomolar affinity for Cu^{2+} allows Aβ to compete for Cu^{2+} ions with other extracellular Cu^{2+} chelators, especially at the synapse during neuronal de-

* This work was supported by Biotechnology and Biological Sciences Research Council (BBSRC) Project Grant BBD0050271 and a BBSRC quota studentship.

[S] The on-line version of this article (available at http://www.jbc.org) contains supplemental Table S1 and Figs. S1–S10.

[1] To whom correspondence should be addressed. Tel.: 44-020-7882-8443; Fax: 44-020-8983-0973; E-mail: j.viles@qmul.ac.uk.

[2] The abbreviations used are: AD, Alzheimer disease; Aβ, amyloid-β-peptide; TEM, transmission electron microscopy; ThT, thioflavin T.

polarization where fluxes of Cu^{2+} are reported to be 20–250 μM (39).

Studies showed more than a decade ago that Zn^{2+} and Cu^{2+} ions cause marked aggregation of Aβ (40, 41). These initial studies did not make the distinction between amorphous aggregates, which are nontoxic to cells, and the formation of amyloid fibers. Further investigations using the fiber specific fluorophore thioflavin T (ThT) suggested that Zn^{2+} and Cu^{2+} only promote amorphous aggregation of Aβ and actually inhibit fiber formation and cell toxicity (42–46). We became interested in the factors that promote self-association of Aβ, the relationship between amorphous aggregation and amyloid fiber formation, and a role for Cu^{2+} ions in promoting fiber formation. Furthermore, we wanted to establish whether there was a link between the influence of Cu^{2+} ions on fiber formation and the effect of Cu^{2+} ions on cell toxicity of Aβ.

EXPERIMENTAL PROCEDURES

Aβ Production and Solubilization—Aβ(1–40) and Aβ(1–42) were synthesized using solid phase Fmoc (*N*-(9-fluorenyl)-methoxycarbonyl) chemistry; the peptides were purchased commercially from ABC-London and Zinisser Analytic. HPLC indicated a single peak with the expected molecular mass. The peptides were also characterized by ^1H NMR, and Met^{35} was confirmed to be unoxidized. Lyophilized Aβ(1–40) and Aβ(1–42) were solubilized by dissolving 0.8 mg/ml Aβ in water at pH 10 and then placed at 5 °C for 72 h. It is clear that Aβ is essentially seed-free as Aβ preparations at pH 7.4 have a lag phase of typically 100 h. The concentration of Aβ was determined using the tyrosine absorbance at 280 nm, $\epsilon_{280} = 1280\ M^{-1}\ cm^{-1}$.

Fiber Growth Assay—The binding of ThT to amyloid fibers was used to monitor the kinetics of amyloid formation. ThT binding to amyloids induces the ThT to fluoresce at 487 nm. This fluorescence signal is related directly to the amount of amyloid. A BMG-Galaxy fluoro-star fluorescence 96-well plate reader was used for the ThT measurements. The central 60 wells were used, whereas wells around the edge contained buffer only, to minimize evaporation effects. Readings were taken every 30 min. The well plates were subjected to 30 s of agitation prior to each fluorescence measurement. Fluorescence excitation was at 440 nm and emission detected at 490 nm.

Fiber growth kinetics are very sensitive to a number of factors that must be carefully controlled. They include the pH, concentration, agitation, temperature, and ionic strength. Solubilization of Aβ into a seed-free form is also important. Fiber growth experiments were incubated at 30 °C in 160 mM NaCl. In addition, 50 mM HEPES buffer was used throughout; HEPES was used for its low affinity for Cu^{2+} and Zn^{2+} ions. Small adjustments were made with 10 mM NaOH or HCl to the stock Aβ solutions. The pH, a critical parameter in fiber growth rates, was measured before and after each fiber growth experiment; variations were 0.05, or fewer, pH units over the course of the experiment. Metal stocks solutions were 25 mM $CuCl_2$ and 20 mM $ZnCl_2$ or as a $Cu(Gly)_2$ chelate. UHQ water ($10^{-18}\ \Omega^{-1}cm^{-1}$ resistivity) was used at all times.

TABLE 1

Kinetic data from fibril growth curves with and without Cu^{2+} present

Data were obtained from fitting Equation 1 (see "Experimental Procedures") to the graphs shown in Fig. 1, with the S.E. shown in parentheses. A, B, and C indicate data obtained in separate experiments. Equation 1 determines the kinetics parameters: $t_{(50)}$, (X_o); $t_{(lag)}$, ($X_0 - 2dx$) and; k_{app}, ($1/dx$) with the number of traces shown in *n*.

Experiment	t_{50} (h)	t_{lag} (h)	k_{app} (h^{-1})	*n*
A				
Apo	72 (2)	55 (3)	0.120 (0.007)	6
0.5 Cu^{2+}	42.6 (0.6)	32.2 (0.8)	0.20 (0.01)	6
B				
Apo	68 (2)	53 (8)	0.09 (0.03)	9
0.5 Cu^{2+}	20 (3)	14 (3)	0.20 (0.06)	8
1.0 Cu^{2+}	41 (3)	28 (3)	0.17 (0.03)	9
C				
Apo	72 (1)	49 (2)	0.091 (0.006)	9
1.0 Cu^{2+}	36 (2)	16 (4)	0.12 (0.02)	8

Growth Curve Analysis—Conversion of essentially monomeric Aβ to fibrillar Aβ follows a characteristic growth curve, typically described as the lag phase (nucleation) and a growth phase (elongation). A number of empirical parameters can be obtained from the fiber growth curve, including the time needed to reach half-maximal ThT intensity (t_{50}) and the lag time (t_{lag}) (see Table 1 and supplemental Table S1. The t_{50} is influenced by both the nucleation and elongation phases. These values can readily be extracted from the data by fitting the growth curve to the following equation (25),

$$Y = (y_i + m_i x) + \frac{(v_f + m_f x)}{(1 + \exp^{-(X - X_{0/\tau})})} \qquad \text{(Eq. 1)}$$

where Y is the fluorescence intensity, x is the time, X_0 is the time at half-height of fluorescence (t_{50}). The apparent fiber growth rate is $K_{app} = 1/\tau$, and the lag time (t_{lag}) is $X_0 - 2\tau$. This equation allows for a slope in the initial and final parts of the growth curve, $(y_i + m_i x)$, $(v_f + m_f x)$, rather than forcing these to be horizontal. The fibril growth curves have also been fitted using an alternative equation to extract a rate of nucleation and elongation (47) shown in supplemental Table S1.

Kinetics parameters have been extracted from between six and nine raw traces. Mean values with 1 S.E. are given in Table 1 and supplemental Table S1. A two-tailed unpaired *t* test was used to confirm the significance of the difference between the kinetics with and without a Cu^{2+} ion.

Transmission Electron Microscopy (TEM)—Aβ samples were freeze-dried and resuspended to obtain a peptide concentration of 0.5 mg/ml. The samples were added to 200-mesh carbon-coated copper grids via the droplet method, and 2% uranyl acetate was used to negatively stain the samples. Images were collected with a JEOL JEM-2010 microscope operating at 200 kV.

Cell Viability—PC12 cells were used to assess the cytotoxic effect of different Aβ preparations (48). Cells were spun down at 95 × *g* for 5 min and resuspended in 1 ml of Opti-MEM. Opti-MEM was used due to its low protein concentration (15 μg/ml total protein concentration) to minimize the presence of potential competing copper chelators. A 10-μl aliquot of the cells was added to 10 μl of 3 mg/ml trypan blue, and the cells were counted. The cell stock was then diluted in Opti-MEM and added to the wells in a 96-well plate to give a typi-

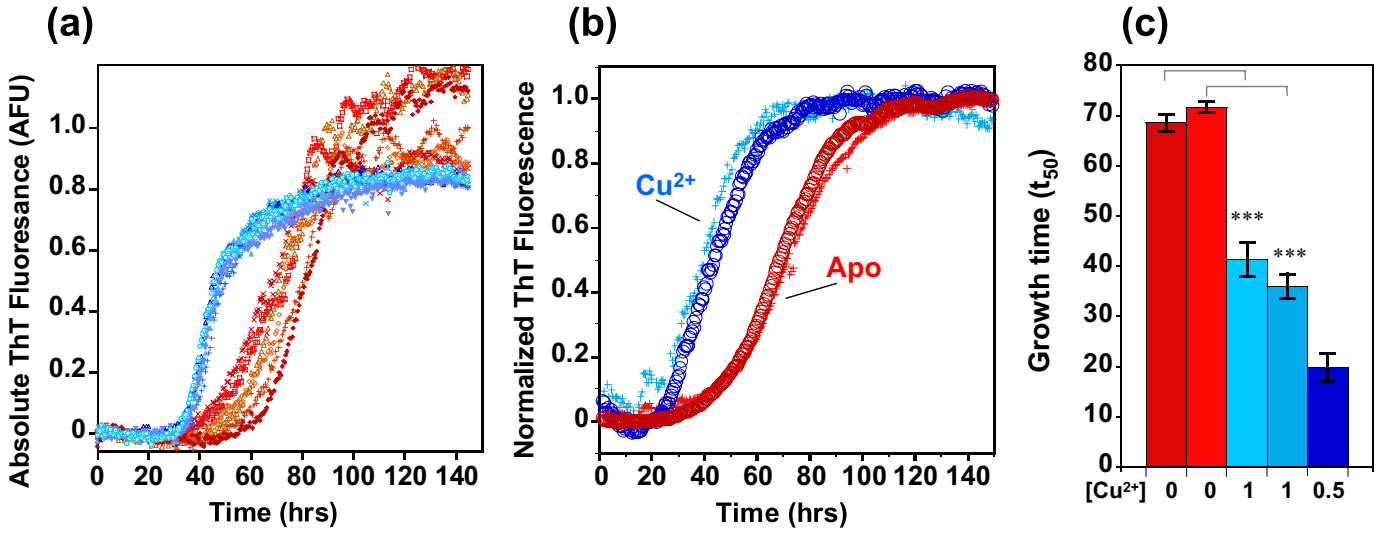

FIGURE 1. **Cu^{2+} accelerates fiber growth.** *a*, fiber growth curves with 0.5 mol eq Cu^{2+} (*blue traces*) and without Cu^{2+} (*red traces*) at pH 7.4. Six traces are shown for each condition, and the ThT fluorescence values are absolute. 5 μM Aβ(1–40), 50 mM HEPES buffer, 160 mM NaCl at 30 °C is shown. *b*, average of nine growth curves recorded on two separate occasions, apo in *red*, 1 mol eq of Cu^{2+} in *blue*. The fluorescence signal is normalized at maximal intensity. *c*, time to reach half-maximal fluorescence (t_{50}) in two experiments with 0 (*red*), 1 (*mid-blue*), or 0.5 (*dark blue*) mol eq of Cu^{2+} ions. The presence of Cu^{2+} typically halves the time taken to form fibers. *Error bars* are for S.E. from nine traces. ***, $p = 0.001$.

cal concentration of 5×10^4 cells/ml, or 1×10^4 cells/well. Typically, cells were incubated with the Aβ preparations, and at various time points, between 1 and 6 days, 10% (v/v) alamarBlue was added. The wells were then incubated at 37 °C for a further 4–6 h to allow color development. The concentration of viable cells present is indicated by alamarBlue fluorescence. The fluorescence was measured in a Molecular Devices SpectraMax Gemini XPS, excitation at 530 nm and emission at 585 nm.

^1H NMR—The pH-dependent protonation state of the three histidine side chains of Aβ were determined from ^1H NMR chemical shifts of the ϵH and δH protons, recorded at 0.5-pH unit intervals between pH 5 and 9, as shown in supplemental Fig. S7. The singlet chemical shifts of the ϵ and δ protons were readily identified from the one-dimensional ^1H NMR spectra. His CϵH and CδH assignments were confirmed using two-dimensional ^1H TOCSY spectra, using standard acquisition parameters and a spin-lock of 60 ms. Assignment of the His^6, His^{13}, and His^{14} residues was based on previous ^1H NMR studies with H6A, H13A, and H14A analogs (49). The Aβ(1–28) fragment was used rather than full-length Aβ(1–40) to improve solubility. 10 μM 4,4-dimethyl-4-silapentane-1-sulfonic acid was used as a reference, 0.1 mM Aβ(1–28) in 50 mM phosphate buffer, in 90% H_2O, 10% D_2O, at 25 °C. The pH-dependent shifts for ϵ and δ protons were fitted to a modified Hill equation to determine pK_a for His^6, His^{13}, and His^{14} and are also presented in supplemental Fig. S7.

RESULTS AND DISCUSSION

$Copper^{2+}$ and Fibril Growth Rates—Using the well established amyloid-binding ThT fluorescence assay, we have investigated fiber formation over a range of Aβ concentrations, with and without the presence of Cu^{2+} ions. Aβ concentrations of >10 μM, pH 7.4, showed no detectable amyloid fibrils in the presence of 1 mol eq of Cu^{2+} ions (see supplemental Fig. S1), as reported previously (42, 43). However, under more dilute conditions, with Aβ between 5 and 2 μM, rapid fiber formation was detected in the presence of Cu^{2+} ions. Fig. 1 shows that Cu^{2+} ions significantly increase the rate of Aβ fiber formation at pH 7.4. In Fig. 1*a*, multiple ThT fluorescence traces are shown, with and without Cu^{2+} ions present, Fig. 1*b* shows normalized data from the mean of nine measurements repeated on two separate occasions (individual fluorescence traces are shown in supplemental Fig. S2). Metal-free Aβ preparations typically take more than 70 ± 2 h to reach half-maximal fluorescence (t_{50}), whereas the same Aβ preparations with 0.5 or 1 mol eq of Cu^{2+} ions cause fibers to form in nearly half the time, 38 ± 2 h (Fig. 1*c*). A two-tailed unpaired *t* test confirms that Cu^{2+} ions significantly increase fiber growth rates with 99.9% confidence. Kinetic parameters taken from the fiber growth curves are given in Table 1 and supplemental Table S1.

Inspection of the growth curves indicates that both the nucleation and elongation rate are accelerated by Cu^{2+} ions for Aβ(1–40). However the lag time is particularly reduced by Cu^{2+} ions, from 49 to 16 h, for example (see Table 1). In the case of Aβ(1–42), elongation rates and total fiber content generated are significantly enhanced by the presence of Cu^{2+} ions (supplemental Fig. S3) whereas the lag times are less affected by Cu^{2+} ions. We have repeated this fiber growth experiment at a number of pH values (8.0, 8.5, and 9.0), and in each case Cu^{2+} increases the rate of fiber formation (supplemental Fig. S4). Studies with Cu^{2+} added as a $Cu(glycine)_2$ chelate produced identical results (supplemental Fig. S5). It is notable that the total ionic strength is unaffected by the Cu^{2+} addition, which is constant at 160 mM NaCl.

We then characterized the nature of the Cu^{2+}-promoted amyloids. TEM images indicate the presence of fibers (Fig. 2). Based on TEM images, under these conditions, the morphology of the fibers generated appears quite similar for fibers formed with and without the presence of Cu^{2+} ions. We note

that previous studies by other groups using TEM did not reveal fibers in the presence of Cu^{2+} because the high Aβ and Cu^{2+} concentrations used caused amorphous precipitation (42–46). Furthermore, the Cu^{2+}-generated fibers are capable of seeding fiber formation of fresh, metal-free Aβ as indicated by a reduction in the lag time (see supplemental Fig. S6).

How does the presence of Cu^{2+} ions accelerate the rate of fiber formation? At μM concentrations of Aβ, Cu^{2+} does not form crossed-linked species (26, 27, 50), and the Cu^{2+} coordination geometry is identical in the monomer and fiber (25, 28). This rules out copper bridging to form cross-linked Aβ as a possible mechanism of accelerated fiber formation. Cu^{2+} coordination may trigger the Aβ misfolding that nucleates fiber assembly; however, the conformational changes in Aβ upon Cu^{2+} binding are small and outside of the fiber core (25, 26). It is, however, well documented that intermolecular self-association is strongly influenced by the net charge of the protein. As Aβ approaches its isoelectric point, a pI of 5.3, and an overall neutral charge, its solubility decreases (51, 52). We investigated the effect of the net charge of Aβ on the rate of fiber formation more quantitatively by varying the pH and monitoring fiber growth. The growth of Aβ fibers over a range of pH values is shown in Fig. 3*a*. It is clear that as the pH drops from 8.3 to 5.9 the rate at which fibers form significantly increases. Fig. 3*b* is a plot of lag times versus pH, lag times (t_{lag}) reduce from 170 (±8) h at pH 8.3 to 23 (±4) h at pH 5.9.

We note that pH dependence of the fiber growth rates bears a strong resemblance to the protonation state of the histidine residues and the N-terminal group within Aβ. For direct comparison we determined the protonation state of the three His residues within Aβ (His^6, His^{13}, and His^{14}) over a range of pH values using ^{1}H NMR chemical shift measurements (Fig. 3*b inset* and supplemental Fig. S7). The pK_a of the His residues at 25 °C is 6.7. It appears the protonation state of the three imidazole rings and the N terminus (pK_a 7.9), and consequently the net charge of Aβ, is crucial to its amyloidogenicity.

In addition to pH, the binding of metal ions will also perturb the net charge of Aβ. It is known that Cu^{2+} (and Zn^{2+}) ions bind to the three histidine residues within Aβ (3, 25–28, 36, 49). At pH 7.4 Aβ histidine residues are predominantly (80%) deprotonated and neutrally charged, thus coordination of a divalent Cu^{2+} (or Zn^{2+}) ion to Aβ histidines adds two positive charges. Adding two positive charges to Aβ at pH 7.4 makes the Aβ peptide complex more neutral in overall net charge, and therefore more prone to self-association, with the result that fiber growth times are almost halved.

The stoichiometric effect of Cu^{2+} on fiber growth was investigated in more detail. All stoichiometries of Cu^{2+} up to 1 mol eq caused the rate of fibrillization to increase. Interestingly, substoichiometric amounts of Cu^{2+} between 0.2 and 0.4 mol eq display the greatest increase in fiber growth rates (Fig. 4). This supports the observation that Cu^{2+} accelerates nucle-

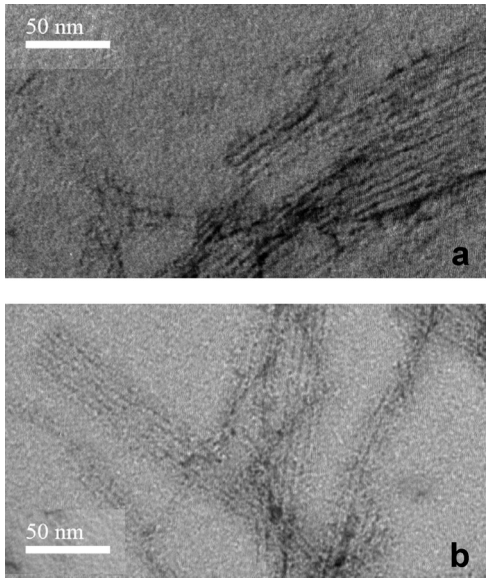

FIGURE 2. **TEM images of Aβ(1–42) fibrils formed in the absence (*a*) and presence (*b*) of Cu^{2+} ions.** The morphologies of fibers formed with and without Cu^{2+} ions present are similar; typically long, straight, unbranched fibers are observed often stacked together. *Scale bar*, is 50 nm. The negatively stained fibers are generated from 3 μM Aβ(1–42) with and without 0.5 mol eq of Cu^{2+} ions, over 200 h with agitation every 30 min, at 30 °C in 50 mM HEPES, 160 mM NaCl. The fibrils were then freeze-dried to ~0.5 mg/ml.

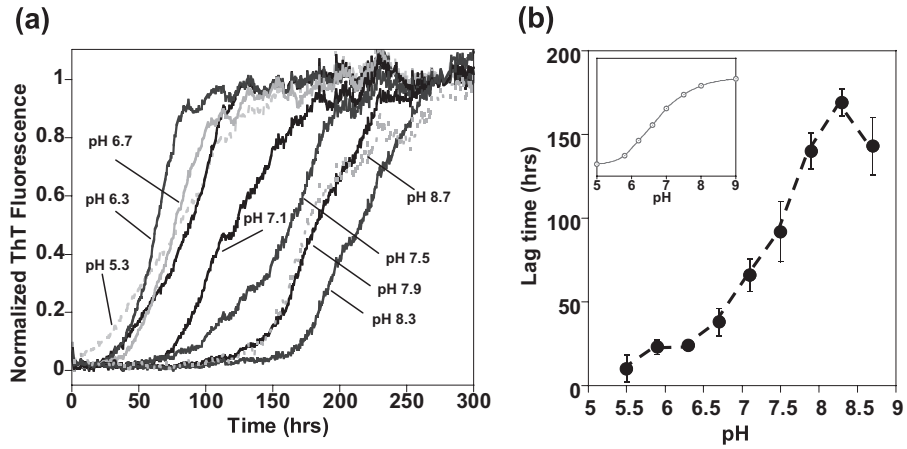

FIGURE 3. **pH dependence of Aβ fiber formation.** *a*, fiber growth curves (average from six traces) between pH 5.5 and 8.7, for Aβ(1–40) at 5 μM with 160 mM NaCl. The maximal ThT fluorescence signal has been normalized. *b*, lag times for fibril growth (t_{lag}) *versus* pH. *Inset*, protonation state of the three histidine residues of Aβ *versus* pH. Data are based on ^{1}H NMR chemical shift. The rate fibers formed increases as Aβ approaches its isoelectric point, and this is dependent on histidine protonation.

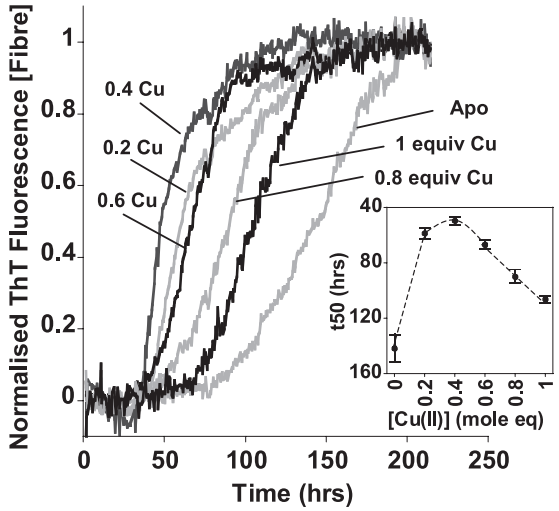

FIGURE 4. **Effect of Cu^{2+} concentration on fibril growth rates.** Normalized fibril growth curves with different mole equivalents of Cu^{2+} ions. The *inset* shows that fiber growth times (t_{50}) all decrease in the presence of Cu^{2+} ions, from 150 h for the apo to 50 h with 0.4 mol eq of Cu^{2+} ions. The maximal effect is between 0.2 and 0.4 mol eq of Cu^{2+}. With excess, 2 and 4 mol eq, of Cu^{2+} ions the fibril growth is completely inhibited. Growth curves represent the mean of six traces. *Error bars* indicate S.E. Aβ(1–40) at 5 μM in 50 mM HEPES, 160 mM NaCl, at pH 7.4, 30 °C, with intermittent agitation is shown.

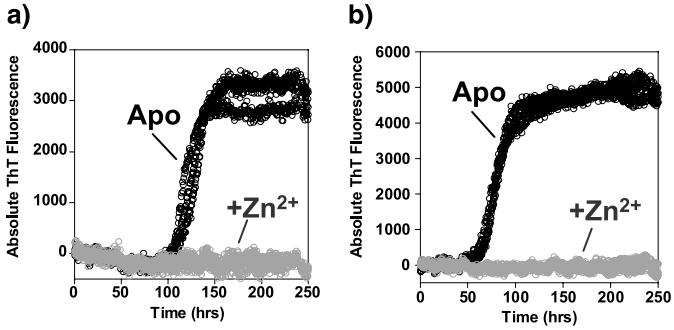

FIGURE 5. **Zn^{2+} inhibits fibril growth.** Fibril growth curves with 1 mol eq of Zn^{2+} ions (*gray*) and metal free (*black*) in (*a*) 3 μM Aβ(1–40), pH 7.4 or (*b*) 4 μM Aβ(1–40), pH 7.4, is shown. The experiment was carried out in 50 mM HEPES, 160 mM NaCl, 30 °C, with agitation. Three to six traces for each experiment are shown.

ation (as well as elongation) as this suggests that substoichiometric amounts of Cu^{2+} can nucleate fiber formation. Further addition of Cu^{2+} beyond 1 mol eq caused precipitation of Aβ and markedly reduced the amount of fibers generated (supplemental Fig. S1), as previously noted (53, 54). The total amount of fibers generated in the presence (or absence) of Cu^{2+} ions can be quite variable (supplemental Fig. S8*a*), presumably reflecting competition between fibril formation and amorphous aggregation. Interestingly, Cu^{2+} ions tend to increase the total amount Aβ(1–42) fiber generated (supplemental Fig. S3). As with the effect of Cu^{2+} ions on Aβ(1–40), it is also notable that at lower pH values the maximal intensity of the ThT fluorescence signal is reduced (supplemental Fig. S8*b*). As the pH drops closer to the pI of Aβ, formation of amorphous aggregates competes with the rapid formation of ordered amyloids (55). This effect is reduced with dilution, but 2–5 μM levels of Aβ are required for reliable timely detection. This concentration-dependent process can be likened to the crystallization of proteins, in which overly precipitative conditions for self-association will cause amorphous aggregates rather than ordered crystals to form. A limitation in previous experiments that showed only amorphous aggregates was the high concentration of Aβ and Cu^{2+} ions used (42, 43) (typically 50 μM, 100 μM, respectively), much higher than that found *in vivo*.

Interestingly, accelerated fibril formation appears to be quite specific for Cu^{2+} ions, Zn^{2+} ions completely inhibit fiber formation even at 3 μM Aβ(1–40) (Fig. 5). This may be due to the very different coordination geometry (at micromolar concentration) between the two metal ions. Cu^{2+} ions form an intramolecular complex with Aβ (25–28) whereas at micromolar levels current data suggest that Zn^{2+} will form an intermolecular complex, cross-linking between histidine residues on multiple Aβ molecules (34, 36, 49, 56). These cross-linked Zn^{2+}-Aβ species will inhibit amyloids forming by interfering with the regular cross-beta assembly.

Copper and Aβ Cell Toxicity—We wanted to relate the ability of Cu^{2+} ions to promote fiber formation of Aβ to the cell toxicity. We have added both monomeric Aβ and fibrillar Aβ to PC12 cells with and without the presence of Cu^{2+} ions. Cu^{2+} ions bound to Aβ are more cytotoxic than Aβ in the absence of Cu^{2+} ions, whereas the same levels of Cu^{2+} in the absence of Aβ are not toxic to the cells. Fig. 6*a* shows that Aβ(1–42) fibers incubated with PC12 cells are toxic (40% viability), whereas generation of Aβ fibers in the presence of Cu^{2+} ions (a half-mol eq in Cu^{2+} ions) makes the Aβ(1–42) fibers considerably more toxic (only 4% viability). This experiment was repeated on a number of occasions, and each time the presence of Cu^{2+} ions consistently enhanced Aβ toxicity to PC12 cells. Control studies show that the same levels of Cu^{2+} ions (2.5 μM) are not toxic to the cells. Supplemental Fig. S9*a* shows that free Cu^{2+} ions over a range of concentrations have no detectable toxic effect; Cu^{2+} ions were added to the cell medium as $CuCl_2$. A further control in which Cu^{2+} was bound to the nonamyloidogenic Cu^{2+}-binding fragment, Aβ(1–16), was studied. Cu^{2+} ions when bound to Aβ(1–16) are not toxic (supplemental Fig. S9*b*), showing that the toxic effects of Cu^{2+} are specific to their interaction with Aβ(1–42) and Aβ(1–40). The use of Aβ(1–16) is a particularly good control as Cu^{2+} binds to the shorter fragment of Aβ with the same affinity and coordination geometry (25–28), but Aβ(1–16) lacks the amyloidogenic region and does not form fibrils.

Next, we were interested in the ratios of Cu^{2+} to Aβ that caused toxicity. As little as 0.01 mol eq of Cu^{2+} (100 nM) was found to be significantly more toxic than Aβ(1–40) fibers in the absence of Cu^{2+} ions (Fig. 6*b*). With 0.1 mol eq of Cu^{2+}, bound Aβ was even more toxic, whereas 0.5 mol eq of Cu^{2+} ions were also more toxic than Aβ(1–40) in the absence of Cu^{2+} ions. However, at the Cu^{2+} ratio of 1:1 mol eq, the toxic effects of Cu^{2+} are lost. Indeed at, 5 mol eq of Cu^{2+}, relative to Aβ(1–40), Cu^{2+} is actually protective (Fig. 6*b*). Interestingly, these observations can be directly related to the optimum ratio of Cu^{2+}-Aβ that generates amyloid fibers, as shown in Fig. 4. We have already shown that substoichiometric amounts of Cu^{2+} (0.2–0.4 mol eq) are more effective at generating amyloid fibers, whereas Cu^{2+} levels above 1 mol

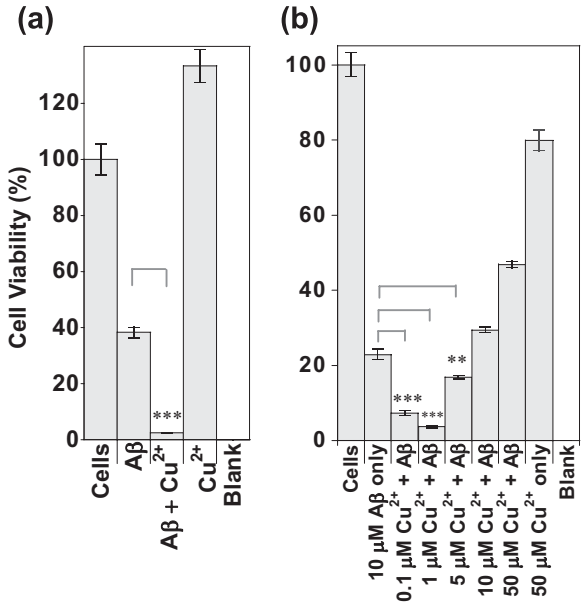

FIGURE 6. **Cell viability, Cu^{2+}-Aβ is more cytotoxic than Aβ.** *a*, Aβ(1–42) as preformed fibrils, 3 μM, with and without the presence of 1.5 μM Cu^{2+} was added to PC12 cells to give a concentration in the well of 2.7 μM Aβ and 1.35 μM Cu^{2+}. Cell concentration was 5.9×10^4 cells/ml. 2.5 μM Cu^{2+} was added to the cells alone to test Cu^{2+} toxicity. *Blank* is buffer only. All preparations were incubated with the cells for 24 h, and then 10% (v/v) alamarBlue was added. The data shown here are after total incubation for 70 h. *b*, 10 μM monomeric Aβ(1–40) with a range of Cu^{2+} concentrations was incubated with PC12 cells for 6 days. AlamarBlue was then added and the reading taken. Cell concentration was 5.4×10^4 cells/ml. All cell experiments were conducted in Opti-MEM, pH 7.4. *Error bars* are S.E., $n = 3$. ***, $p = 0.001$; **, $p = 0.02$.

eq will actually inhibit fiber formations (supplemental Fig. S1*b*). Clearly, the influence of Cu-Aβ ratios on Aβ toxicity relate closely to the ability of Cu^{2+} to accelerate (or inhibit) fiber formation.

Both preformed fibrils (Fig. 6*a*) and Aβ added as a monomer (Fig. 6*b*) are toxic to cells. The toxic effects of fibrillar Aβ are apparent within a day of addition to the cell medium. However, addition of monomeric Aβ(1–40) shows no significant cell cytotoxicity within 2 days of incubation; it is only after this time that the toxic effects are apparent. Fiber growth in the cell medium, detected using a ThT assay, suggests that fibers will take a few days to form, supporting the hypothesis that cytotoxicity observed correlates with the rate at which Aβ fibers are generated.

Over a range of concentrations of fibrillar Aβ(1–42), Cu^{2+} ions increase Aβ toxic effects, shown in supplemental Fig. S10. Counterintuitively, at lower Aβ(1–42) concentrations a greater toxic effect is observed. We suggest that a larger amount of toxic species is present because more protofibrils and fewer amorphous aggregates are generated, at the more dilute concentrations of Aβ(1–42). Interestingly, Aβ(1–42) at 4.5 μM has almost no toxic effect; 89 (±14)% viability is observed. The addition of Cu^{2+} ions Aβ(1–42) becomes markedly toxic with 19 (±0.4)% cell viability.

There are a few studies already published investigating the relationship between copper and Aβ cell toxicity (19, 20, 24, 42). These studies appear to show conflicting results; in one study copper promoted toxicity (19), and in another it appeared to protect against toxicity (42). In these studies the nature of the Aβ preparation was not well defined (*i.e.* amorphous aggregate, monomer or fiber), and this may be the source of the discrepancies. Here we are able to correlate the kinetics of fibril formation in the presence of Cu^{2+} ions with the severity of cytotoxicity. The levels of Cu^{2+} used relative to Aβ can now explain contradictory observations in the literature. This effect is highlighted in Fig. 6*b* where substoichiometric levels of Cu^{2+} significantly reduce cell viability, whereas suprastoichiometric levels are actually protective. Clearly, lower substoichiometric levels of Cu^{2+} are the more physiologically relevant case, suggesting a role for Cu^{2+} ions in enhancing Aβ toxicity.

There are potentially two reasons for the enhanced toxicity of Aβ in the presence of Cu^{2+} ions. Diffusible oligomers of Aβ could bind Cu^{2+}, resulting in a concentration of Cu^{2+} ions at the neuronal cell surface, where Cu^{2+} would generate toxic hydrogen peroxide and hydroxyl radicals. Indeed, Aβ oligomers are found clustered at synaptic terminals (57) and cause memory loss due to synapse failure (58). Redox-active Cu^{2+} ions released at synaptic terminals will cause lipid peroxidation at the cell membrane and so compromise cell integrity (19, 21, 59), leading to the neuron loss characteristic of AD. The observation that the antioxidant protein catalase and the Cu^{2+} chelator metallothionein III are protective strongly supports this hypothesis (18–20, 24). Alternatively, the Cu^{2+} ions could promote the formation of protofibrillar/fibrillar Aβ species that are toxic to the cells. The rate of production, quantity, or morphology of the Cu^{2+}-promoted fibers and protofibrillar oligomers may cause the heightened cytotoxicity. We conclude that if it was simply a matter of reactive oxygen species generation by Cu^{2+} ions bound to Aβ then one might expect the more Cu^{2+} present, the greater the toxicity; however, in Fig. 6*b* we observe that small amounts of Cu^{2+} ions (0.1 μM) are more toxic than 50 times as much (5 μM) Cu^{2+} ions. Thus, the ability of Cu^{2+} to promote fibers (and by inference protofibrillar species) appears to be the significant factor in reactive oxygen species promoted Aβ cell toxicity.

CONCLUSIONS

Cu^{2+}-Aβ is more toxic to PC12 cells than Aβ on its own; furthermore, cytotoxic effects are related to the ability of Cu^{2+} ions to promote amyloid fibers and protofibrils. We suggest that Cu^{2+} ions increase the rate of fiber formation, at pH 7.4, by causing Aβ to approach its isoelectric point. To put our observation in context, the increase in fiber growth rates measured here due to Cu^{2+} ions is comparable with that observed for (metal-free) Aβ(1–40) mutants associated with familial early onset AD (E22K/G/Q), where a halving of the growth times (t_{50}) of fiber formation is also reported (60). Metals have also been proposed as triggers for other misfolding and assembly diseases such as dialysis-related amyloidosis (61), Parkinson disease (62), and prion diseases (63, 64), although it remains to be established whether the mechanisms by which metals induce fibrillization are shared. Our observations provide a rationale for the *in vivo* observations in *Drosophilia* and mammals which link the AD phenotype with impaired Cu^{2+} homeostasis (6, 7). It is known that Cu^{2+} levels in the brain increase with age (2); thus, our observations

should refocus attention on loss of Cu^{2+} homeostasis as a possible risk factor in AD. Cu^{2+} chelators are being investigated in clinical trials as a potential therapy for AD (2, 65, 66).

Acknowledgments—We thank Harold Toms for assistance with NMR, John Nield and Zofia Luklinska for assistance with TEM, and Henry Clarke and Neveen Hosny for assistance with growth curve analysis.

REFERENCES

1. Hardy, J., and Selkoe, D. J. (2002) *Science* **297,** 353–356
2. Barnham, K. J., and Bush, A. I. (2008) *Curr. Opin. Chem. Biol.* **12,** 222–228
3. Dong, J., Atwood, C. S., Anderson, V. E., Siedlak, S. L., Smith, M. A., Perry, G., and Carey, P. R. (2003) *Biochemistry* **42,** 2768–2773
4. Lovell, M. A., Robertson, J. D., Teesdale, W. J., Campbell, J. L., and Markesbery, W. R. (1998) *J. Neurol. Sci.* **158,** 47–52
5. Miller, L. M., Wang, Q., Telivala, T. P., Smith, R. J., Lanzirotti, A., and Miklossy, J. (2006) *J. Struct. Biol.* **155,** 30–37
6. Sanokawa-Akakura, R., Cao, W., Allan, K., Patel, K., Ganesh, A., Heiman, G., Burke, R., Kemp, F. W., Bogden, J. D., Camakaris, J., Birge, R. B., and Konsolaki, M. (2010) *PLoS One* **5,** e8626
7. Sparks, D. L., and Schreurs, B. G. (2003) *Proc. Natl. Acad. Sci. U.S.A.* **100,** 11065–11069
8. Phinney, A. L., Drisaldi, B., Schmidt, S. D., Lugowski, S., Coronado, V., Liang, Y., Horne, P., Yang, J., Sekoulidis, J., Coomaraswamy, J., Chishti, M. A., Cox, D. W., Mathews, P. M., Nixon, R. A., Carlson, G. A., St. George-Hyslop, P., and Westaway, D. (2003) *Proc. Natl. Acad. Sci. U.S.A.* **100,** 14193–14198
9. Bayer, T. A., Schäfer, S., Simons, A., Kemmling, A., Kamer, T., Tepest, R., Eckert, A., Schüssel, K., Eikenberg, O., Sturchler-Pierrat, C., Abramowski, D., Staufenbiel, M., and Multhaup, G. (2003) *Proc. Natl. Acad. Sci. U.S.A.* **100,** 14187–14192
10. Crouch, P. J., Hung, L. W., Adlard, P. A., Cortes, M., Lal, V., Filiz, G., Perez, K. A., Nurjono, M., Caragounis, A., Du, T., Laughton, K., Volitakis, I., Bush, A. I., Li, Q. X., Masters, C. L., Cappai, R., Cherny, R. A., Donnelly, P. S., White, A. R., and Barnham, K. J. (2009) *Proc. Natl. Acad. Sci. U.S.A.* **106,** 381–386
11. Yankner, B. A., and Lu, T. (2009) *J. Biol. Chem.* **284,** 4755–4759
12. Glabe, C. G. (2008) *J. Biol. Chem.* **283,** 29639–29643
13. Meyer-Luehmann, M., Spires-Jones, T. L., Prada, C., Garcia-Alloza, M., de Calignon, A., Rozkalne, A., Koenigsknecht-Talboo, J., Holtzman, D. M., Bacskai, B. J., and Hyman, B. T. (2008) *Nature* **451,** 720–724
14. Urbanc, B., Cruz, L., Le, R., Sanders, J., Ashe, K. H., Duff, K., Stanley, H. E., Irizarry, M. C., and Hyman, B. T. (2002) *Proc. Natl. Acad. Sci. U.S.A.* **99,** 13990–13995
15. Roychaudhuri, R., Yang, M., Hoshi, M. M., and Teplow, D. B. (2009) *J. Biol. Chem.* **284,** 4749–4753
16. Butterfield, D. A., Reed, T., Newman, S. F., and Sultana, R. (2007) *Free Radic. Biol. Med.* **43,** 658–677
17. Rival, T., Page, R. M., Chandraratna, D. S., Sendall, T. J., Ryder, E., Liu, B., Lewis, H., Rosahl, T., Hider, R., Camargo, L. M., Shearman, M. S., Crowther, D. C., and Lomas, D. A. (2009) *Eur. J. Neurosci.* **29,** 1335–1347
18. Behl, C., Davis, J. B., Lesley, R., and Schubert, D. (1994) *Cell* **77,** 817–827
19. Opazo, C., Huang, X., Cherny, R. A., Moir, R. D., Roher, A. E., White, A. R., Cappai, R., Masters, C. L., Tanzi, R. E., Inestrosa, N. C., and Bush, A. I. (2002) *J. Biol. Chem.* **277,** 40302–40308
20. Huang, X., Atwood, C. S., Hartshorn, M. A., Multhaup, G., Goldstein, L. E., Scarpa, R. C., Cuajungco, M. P., Gray, D. N., Lim, J., Moir, R. D., Tanzi, R. E., and Bush, A. I. (1999) *Biochemistry* **38,** 7609–7616
21. Nadal, R. C., Rigby, S. E., and Viles, J. H. (2008) *Biochemistry* **47,** 11653–11664
22. Barnham, K. J., Haeffner, F., Ciccotosto, G. D., Curtain, C. C., Tew, D., Mavros, C., Beyreuther, K., Carrington, D., Masters, C. L., Cherny, R. A., Cappai, R., and Bush, A. I. (2004) *FASEB J.* **18,** 1427–1429
23. Hureau, C., and Faller, P. (2009) *Biochimie* **91,** 1212–1217
24. Meloni, G., Sonois, V., Delaine, T., Guilloreau, L., Gillet, A., Teissié, J., Faller, P., and Vasák, M. (2008) *Nat. Chem. Biol.* **4,** 366–372
25. Sarell, C. J., Syme, C. D., Rigby, S. E., and Viles, J. H. (2009) *Biochemistry* **48,** 4388–4402
26. Syme, C. D., Nadal, R. C., Rigby, S. E., and Viles, J. H. (2004) *J. Biol. Chem.* **279,** 18169–18177
27. Drew, S. C., Noble, C. J., Masters, C. L., Hanson, G. R., and Barnham, K. J. (2009) *J. Am. Chem. Soc.* **131,** 1195–1207
28. Karr, J. W., and Szalai, V. A. (2008) *Biochemistry* **47,** 5006–5016
29. Shin, B. K., and Saxena, S. (2008) *Biochemistry* **47,** 9117–9123
30. Damante, C. A., Osz, K., Nagy, Z., Pappalardo, G., Grasso, G., Impellizzeri, G., Rizzarelli, E., and Sovago, I. (2008) *Inorg. Chem.* **47,** 9669–9683
31. Hou, L., and Zagorski, M. G. (2006) *J. Am. Chem. Soc.* **128,** 9260–9261
32. Streltsov, V. A., Titmuss, S. J., Epa, V. C., Barnham, K. J., Masters, C. L., and Varghese, J. N. (2008) *Biophys. J.* **95,** 3447–3456
33. Antzutkin, O. N. (2004) *Magn. Reson. Chem.* **42,** 231–246
34. Minicozzi, V., Stellato, F., Comai, M., Serra, M. D., Potrich, C., Meyer-Klaucke, W., and Morante, S. (2008) *J. Biol. Chem.* **283,** 10784–10792
35. Dorlet, P., Gambarelli, S., Faller, P., and Hureau, C. (2009) *Angew Chem. Int. Ed. Engl.* **48,** 9273–9276
36. Faller, P., and Hureau, C. (2008) *Dalton Trans.* **2008,** 1080–1094
37. Faller, P. (2009) *ChemBioChem* **10,** 2837–2845
38. Vigo-Pelfrey, C., Lee, D., Keim, P., Lieberburg, I., and Schenk, D. B. (1993) *J. Neurochem.* **61,** 1965–1968
39. Kardos, J., Kovács, I., Hajós, F., Kálmán, M., and Simonyi, M. (1989) *Neurosci. Lett.* **103,** 139–144
40. Bush, A. I., Pettingell, W. H., Multhaup, G., d Paradis, M., Vonsattel, J. P., Gusella, J. F., Beyreuther, K., Masters, C. L., and Tanzi, R. E. (1994) *Science* **265,** 1464–1467
41. Atwood, C. S., Moir, R. D., Huang, X., Scarpa, R. C., Bacarra, N. M., Romano, D. M., Hartshorn, M. A., Tanzi, R. E., and Bush, A. I. (1998) *J. Biol. Chem.* **273,** 12817–12826
42. Yoshiike, Y., Tanemura, K., Murayama, O., Akagi, T., Murayama, M., Sato, S., Sun, X., Tanaka, N., and Takashima, A. (2001) *J. Biol. Chem.* **276,** 32293–32299
43. Raman, B., Ban, T., Yamaguchi, K., Sakai, M., Kawai, T., Naiki, H., and Goto, Y. (2005) *J. Biol. Chem.* **280,** 16157–16162
44. Ha, C., Ryu, J., and Park, C. B. (2007) *Biochemistry* **46,** 6118–6125
45. Tõugu, V., Karafin, A., Zovo, K., Chung, R. S., Howells, C., West, A. K., and Palumaa, P. (2009) *J. Neurochem.* **110,** 1784–1795
46. Innocenti, M., Salvietti, E., Guidotti, M., Casini, A., Bellandi, S., Foresti, M. L., Gabbiani, C., Pozzi, A., Zatta, P., and Messori, L. (2010) *J. Alzheimers Dis.* **19,** 1323–1329
47. Morris, A. M., Watzky, M. A., Agar, J. N., and Finke, R. G. (2008) *Biochemistry* **47,** 2413–2427
48. Simakova, O., and Arispe, N. J. (2007) *J. Neurosci.* **27,** 13719–13729
49. Syme, C. D., and Viles, J. H. (2006) *Biochim. Biophys. Acta* **1764,** 246–256
50. Talmard, C., Guilloreau, L., Coppel, Y., Mazarguil, H., and Faller, P. (2007) *ChemBioChem* **8,** 163–165
51. Hortschansky, P., Schroeckh, V., Christopeit, T., Zandomeneghi, G., and Fändrich, M. (2005) *Protein Sci.* **14,** 1753–1759
52. Guo, M., Gorman, P. M., Rico, M., Chakrabartty, A., and Laurents, D. V. (2005) *FEBS Lett.* **579,** 3574–3578
53. Smith, D. P., Ciccotosto, G. D., Tew, D. J., Fodero-Tavoletti, M. T., Johanssen, T., Masters, C. L., Barnham, K. J., and Cappai, R. (2007) *Biochemistry* **46,** 2881–2891
54. Jun, S., Gillespie, J. R., Shin, B. K., and Saxena, S. (2009) *Biochemistry* **48,** 10724–10732
55. Wood, S. J., Maleeff, B., Hart, T., and Wetzel, R. (1996) *J. Mol. Biol.* **256,** 870–877
56. Miller, Y., Ma, B., and Nussinov, R. (2010) *Proc. Natl. Acad. Sci. U.S.A.* **107,** 9490–9495
57. Lacor, P. N., Buniel, M. C., Chang, L., Fernandez, S. J., Gong, Y., Viola, K. L., Lambert, M. P., Velasco, P. T., Bigio, E. H., Finch, C. E., Krafft,

G. A., and Klein, W. L. (2004) *J. Neurosci.* **24,** 10191–10200
58. Walsh, D. M., Klyubin, I., Fadeeva, J. V., Cullen, W. K., Anwyl, R., Wolfe, M. S., Rowan, M. J., and Selkoe, D. J. (2002) *Nature* **416,** 535–539
59. Murray, I. V., Sindoni, M. E., and Axelsen, P. H. (2005) *Biochemistry* **44,** 12606–12613
60. Murakami, K., Irie, K., Morimoto, A., Ohigashi, H., Shindo, M., Nagao, M., Shimizu, T., and Shirasawa, T. (2003) *J. Biol. Chem.* **278,** 46179–46187
61. Calabrese, M. F., Eakin, C. M., Wang, J. M., and Miranker, A. D. (2008) *Nat. Struct. Mol. Biol.* **15,** 965–971
62. Uversky, V. N., Li, J., and Fink, A. L. (2001) *J. Biol. Chem.* **276,** 44284–44296
63. Brown, D. R., Qin, K., Herms, J. W., Madlung, A., Manson, J., Strome, R., Fraser, P. E., Kruck, T., von Bohlen, A., Schulz-Schaeffer, W., Giese, A., Westaway, D., and Kretzschmar, H. (1997) *Nature* **390,** 684–687
64. Klewpatinond, M., Davies, P., Bowen, S., Brown, D. R., and Viles, J. H. (2008) *J. Biol. Chem.* **283,** 1870–1881
65. Cherny, R. A., Atwood, C. S., Xilinas, M. E., Gray, D. N., Jones, W. D., McLean, C. A., Barnham, K. J., Volitakis, I., Fraser, F. W., Kim, Y., Huang, X., Goldstein, L. E., Moir, R. D., Lim, J. T., Beyreuther, K., Zheng, H., Tanzi, R. E., Masters, C. L., and Bush, A. I. (2001) *Neuron* **30,** 665–676
66. Crouch, P. J., White, A. R., and Bush, A. I. (2007) *FEBS J.* **274,** 3775–3783